Liquid Crystals
Publication details, including instructions for authors and subscription information:
http://www.informaworld.com/smpp/title~content=t713926090

The pumping phenomenon in smectic C* liquid crystals

I. W. Stewart[a]
[a] Department of Mathematics and Statistics, University of Strathclyde, Glasgow, UK

Online publication date: 06 July 2010

To cite this Article Stewart, I. W.(2010) 'The pumping phenomenon in smectic C* liquid crystals', Liquid Crystals, 37: 6, 799 — 809
To link to this Article: DOI: 10.1080/02678292.2010.492714
URL: http://dx.doi.org/10.1080/02678292.2010.492714

Liquid Crystals,
Vol. 37, Nos. 6–7, June–July 2010, 799–809

Taylor & Francis
Taylor & Francis Group

INVITED ARTICLE

The pumping phenomenon in smectic C* liquid crystals

I.W. Stewart*

Department of Mathematics and Statistics, University of Strathclyde, Glasgow, UK

(*Received 4 May 2010; accepted 7 May 2010*)

It is known from experiments that smectic C* liquid crystals arranged in a bookshelf geometry between two parallel glass plates can exhibit a pumping phenomenon under the application of an electric field when the lower plate is fixed and the upper plate is allowed the possibility of some movement. This phenomenon, which reflects a change in the cell thickness via mechanical vibrations of the top plate, is known to occur when the direction of an applied electric field is suddenly reversed. An elementary model is developed that describes some of the key features of this effect and is directly relevant to the observations reported in the literature. Two aspects are considered: first, the effect of a simple field reversal, and secondly, the frequency-induced effects of an alternating electric field. A steady increase in the cell thickness occurs under alternating fields and this reflects a pumping phenomenon as the director orientation couples to the flow.

Keywords: ferroelectric liquid crystals; smectic liquid crystals; pumping; backflow

1. Introduction

There has been great interest in recent years in ferroelectric liquid crystals, largely due to the possible linear coupling between the spontaneous polarisation and the electric field [1]. It is this coupling, combined with flow, that will be investigated here in relation to reported experiments on the electromechanical effects that arise via flow-induced movements of the liquid crystal boundary plates.

It is known that bookshelf aligned ferroelectric smectic C* (SmC*) liquid crystal samples can exhibit lateral mechanical vibrations under the influence of an applied alternating electric field when the lower sample plate is fixed and the upper plate is free to move, as reported by Jákli *et al.* [2], Jákli and Saupe [3] and Jákli [4]. These vibrations are parallel to both the smectic layers and the boundary plates and perpendicular to the electric field. When both plates are fixed, Zou and Clark [5] observed that a pumping flow of the SmC* liquid crystal can be induced by an alternating electric field: the liquid crystal has flow parallel to the boundary plates within the planes of the smectic layers. There is also a similar pumping phenomenon discovered by Jákli and Saupe [6] that can lead to a steady increase in the sample thickness when the upper plate is free to move and the applied alternating field is above a critical frequency; in contrast to the aforementioned references, when this happens the upper plate vibrates predominantly vertically rather than laterally and a steady increase in the vertical sample thickness occurs and is maintained as fluid is pumped in the direction of the oscillating field. Jákli and Saupe [7] reported that vertical vibrations can also be induced by a fast electric field reversal and it is this phenomenon that is to be modelled here. A simple fast field reversal is first considered and then the effects of an alternating field are explored. The model equations may be adapted [8] to refine the continuum model used in [6] in order to deliver on explanation for what must be a non-zero time average of the pressure, a result which was absent in [6] because the coupling of the director motion to flow was neglected. The work described here delivers a non-zero time average for the pressure when flow is incorporated.

Section 2 describes the model problem. The two main governing equations, 28 and 29, are derived in Section 3 while solutions and comparisons with experimental data are presented in Section 4. The article closes with a discussion of the results in Section 5.

2. Model description

The description of SmC* liquid crystals will follow the standard notation used in [9, 10]. The average orientation of the molecular long axes of a liquid crystal is described by the unit vector **n**, called the director. SmC* liquid crystals are known to form equidistant layers where the director **n** within each layer is tilted by an angle θ with respect to the unit layer normal **a**, as shown in Figure 1(a), which displays the set-up of what is commonly called a smectic bookshelf alignment when the smectic layers are arranged

*Email: i.w.stewart@strath.ac.uk

ISSN 0267-8292 print/ISSN 1366-5855 online

DOI: 10.1080/02678292.2010.492714
http://www.informaworld.com

perpendicular to the boundary plates. The director can maintain this relative tilt to the smectic layers while being free to rotate around the surface of a fictitious cone of semi-vertical angle θ, referred to as the smectic cone angle, shown in Figure 1(b).

It will be assumed throughout that θ is a fixed constant so that the incompressible smectic continuum theory of Leslie *et al.* [11] is applicable. This is motivated by the observations in [5, 6] where the smectic interlayer spacing remained fixed. It is mathematically convenient to introduce two other vectors for a complete description of a SmC* liquid crystal: a unit vector **c**, often called the *c*-director, which is the unit orthogonal projection of **n** onto the smectic planes, and the unit vector $\mathbf{b} = \mathbf{a} \times \mathbf{c}$. Ferroelectric liquid crystals are chiral liquid crystals that have a twist axis perpendicular to the smectic layers and, in general, they possess a spontaneous polarisation, **P**, which, in terms of the model introduced here and displayed in Figure 1(b), can be written as a vector parallel to the vector **b**, so that

$$\mathbf{P} = P_0\mathbf{b}, \qquad P_0 > 0, \tag{1}$$

when the sign of P_0 is taken to be positive, following the usual sign convention of Clark and Lagerwall [12]. It will always be assumed in this article that $P_0 > 0$ for the SmC* material under discussion; in these circumstances, **P** will prefer to align parallel with a positive electric field, as detailed later. The vectors **b** and **c** are orthogonal to each other and always lie in the plane of the smectic layers, perpendicular to **a** as shown in Figure 1(b). In the absence of dislocations it is well-known that the smectic layer normal, **a**, is subject to the constraint $\nabla \times \mathbf{a} = 0$ [13]. This constraint is automatically satisfied when $\mathbf{a} = \hat{\mathbf{x}}$ for planar layers as pictured in Figure 1(a). For fixed planar aligned layers the orientation of the *c*-director can be described by introducing the phase angle ϕ, which is defined to be the angle between the *c*-director and the *y*-axis measured in the positive direction, as shown in Figure 1. For the model equations introduced in the next section, it will be supposed that ϕ is a function of time only. The continuum theory uses the vectors **a** and **c** and thereby provides a complete description for the alignment of **P** since its orientation angle relative to the *y*-axis is always $\phi + \pi/2$ rad in this framework.

The problem to be investigated consists of a bookshelf arrangement of the smectic layers depicted in Figure 1(a) that has been motivated by the experimental results described in [4, 6, 7]. The smectic layers are perpendicular to two parallel glass plates placed initially at a sample depth, h_0, apart in the *z*-direction, **a** being parallel with the *x*-axis. The lower plate is fixed and the upper plate is free to move. The width of the sample in the *y*-direction is initially w_0 and the sample depth in the *x*-direction will be assumed fixed at x_0. Initially, an electric field is applied across the plates in the negative *z*-direction as shown in Figure 1(c), where it is supposed in this problem that the ferroelectric liquid crystal will be in its unwound state, that is, its inherent helical pitch is suppressed by a field of a suitable magnitude that essentially allows the (quadratic) dielectric electric field contribution to be neglected yet permits a linear electric field response linked to **P**, as will be seen later. One possible initial equilibrium state at time $t = 0$ is shown in Figure 1(c) where the electric field is $\mathbf{E} = -E\hat{\mathbf{z}}$ with $E = |\mathbf{E}|$ and $\phi = \pi$. For $t > 0$ the electric field is then reversed so that $\mathbf{E} = E\hat{\mathbf{z}}$. This can lead to a field-induced change in the sample as shown schematically in Figure 2 for a single representative smectic layer.

The initial representative layer at $t = 0$ has height h_0 and width w_0, as pictured in Figure 2(a). The liquid crystal has a fixed smectic interlayer spacing and the fluid is assumed to be incompressible. If the height of

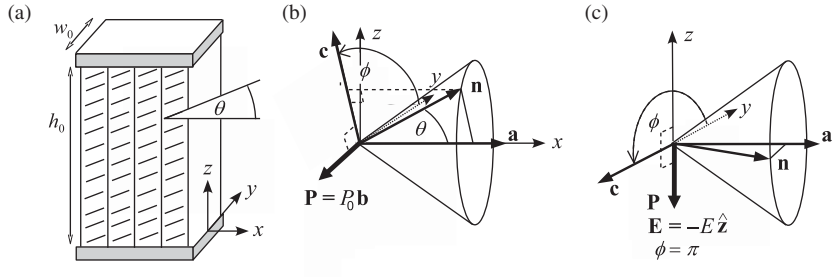

Figure 1. (a) The unwound structure of a bookshelf aligned SmC* liquid crystal. The short, bold lines represent the local alignment of the director when it is tilted at a fixed angle θ relative to the local smectic layer normal. (b) The local geometrical description of the director **n**, layer normal **a**, spontaneous polarisation **P** and the vector **c**, the unit orthogonal projection of the director upon the smectic planes. **n** is tilted at a fixed angle θ to the layer normal $\mathbf{a} = \hat{\mathbf{x}}$. The angle ϕ describes the orientation of **c** within the plane of the layers relative to the *y*-axis. (c) One possible initial configuration when an electric field is applied in the negative *z*-direction so that **P** is aligned with the field and the corresponding orientation angle of **c** is $\phi = \pi$.

the smectic layer increases or decreases then the width must decrease or increase accordingly in order to preserve the volume after a field reversal. Effectively, per unit depth in the x-direction, the area of the smectic layer must remain constant in order to maintain the same volume of material. To a first approximation, the area shapes before and after a field reversal can be assumed to be rectangular. Any changes in height and width will be driven by flow effects coupled to the reorientation of the polarisation with the electric field and will be detected as vertical vibrational displacements to the upper boundary plate. The changes to the height and width may be represented by $h_0 + h(t)$ and $w_0 - w(t)$, respectively, where $h(t)$ and $w(t)$ are zero at $t = 0$. Incompressibility therefore leads to the area in both of the layers pictured in Figure 2 being preserved. These time-dependent functions are, therefore, related and $w(t)$ can be expressed in terms of $h(t)$ through the relation

$$w(t) = \frac{w_0 h(t)}{h_0 + h(t)}. \tag{2}$$

The governing dynamic equations will be derived in the next section. It will turn out that there are three equations to consider: two from the liquid crystal dynamics and one that arises from a boundary condition that involves the movement of the upper boundary plate. Of these, one of the liquid crystal equations will be satisfied by the determined solution for the pressure, p, which leaves two remaining equations to be solved simultaneously for the two unknown functions, $h(t)$ and $\phi(t)$.

3. Governing equations

The basic dynamic theory for SmC liquid crystals was derived by Leslie *et al.* [11] and this theory was subsequently developed further and interpreted for both SmC and SmC* by Carlsson *et al.* [14]. It has been noted by Jákli *et al.* [2] that, for the electromechanical behaviour mentioned above, a continuum theory of fluids should be used in which the viscous behaviour of the material plays a more important role then the elastic properties, an approach that was also adopted effectively in the model equations used by Jákli and Saupe [6]. Motivated by these experimental observations, the elastic effects and boundary conditions for the director may be neglected in a preliminary investigation such as this. Following the model descriptions in Figures 1 and 2, under these circumstances for time $t \geq 0$ it is possible to set

$$\mathbf{a} = (1, 0, 0), \tag{3}$$

$$\mathbf{c} = (0, \cos\phi, \sin\phi), \tag{4}$$

$$\mathbf{b} = (0, -\sin\phi, \cos\phi), \tag{5}$$

$$\mathbf{E} = E(0, 0, 1), \tag{6}$$

where $\phi = \phi(t)$. An example of an initial equilibrium state is shown in Figure 1(c) and occurs when $\phi \equiv \pi$ with $\mathbf{E} = -E\hat{\mathbf{z}}$ so that $\mathbf{P} = -P_0\hat{\mathbf{z}}$ before a field reversal to $\mathbf{E} = E\hat{\mathbf{z}}$ takes place. It will be supposed that the velocity $\mathbf{v}$ may take the form

$$\mathbf{v} = (0, k(t)y, -k(t)z), \tag{7}$$

where $k(t)$ is the time-dependent shear rate that is to be determined. This ansatz for the velocity has been motivated by the review by Leslie [15] and the work of Clark *et al.* [16] that examined oscillatory shear effects in nematic liquid crystals. This form for the velocity satisfies the usual incompressibility condition $\nabla \cdot \mathbf{v} = 0$ and obeys the symmetry requirements that fit with the geometrical description shown in Figure 2(b). For example, the flow component along the y-axis is odd in y, as is to be anticipated if both of the vertical boundaries of a smectic layer are to contract or expand by equal amounts at the same time. The two unknown functions to be determined in the model are, therefore, the angle, $\phi(t)$, and the shear rate, $k(t)$. However, the vertical velocity of the upper plate at $z = h_0 + h(t)$ is clearly given by dh/dt and so this boundary condition allows the shear rate to be expressed in terms of $h(t)$ and its derivative via the requirement

$$k(t) = -\frac{dh}{dt}[h_0 + h(t)]^{-1}. \tag{8}$$

Thus solutions to the problem can be expressed in terms of the orientation angle $\phi(t)$ of the c-director and the vertical displacement $h(t)$ of the upper boundary plate, quantities that are directly relevant to experimental observations via the representation in Figure 2, bearing in mind that $w(t)$ can be determined through the relation 2. The ansatz for the z-component of the velocity, v_3, satisfies the usual no-slip boundary condition at $z = 0$ and matches the velocity of the upper plate at $z = h_0 + h(t)$, as is to be expected. However, the y-component of the velocity is not necessarily zero at the boundary plates in this ansatz. Nevertheless, this may not be a major concern since the velocity obeys an acceptable symmetry across the xz-plane and serves as a fair approximate form for the anticipated flow behaviour. It is also noted here that when flow couples to the director orientation it is often referred to as backflow in the liquid crystal literature.

The incompressible dynamic theory for SmC* [10, 11] requires that **a**, **b** and **c** are mutually orthogonal unit vectors with $\nabla \times \mathbf{a} = 0$ and that the velocity satisfies the incompressibility requirement $\nabla \cdot \mathbf{v} = 0$. All of these constraints are satisfied in this model. The remaining dynamic equations of relevance are those arising from the balance of linear momentum and the balance of angular momentum related to the *c*-director; the remaining angular momentum balance, related to the layer normal, is easily fulfilled by a suitable selection of vector Lagrange multiplier because the layers are fixed, obtained by the method outlined in [10, p266]. The usual Cartesian suffix notation will be used, where a comma denotes partial differentiation with respect to the variable it precedes and repeated suffixes are summed from 1 to 3. The general linear momentum balance equation in the absence of director gradients can be obtained directly from the general theory [10, 11] and is given by

$$\rho \dot{v}_i = \rho F_i - p_{,i} + \tilde{t}_{ij,j}\,, \tag{9}$$

where ρ is the density of the liquid crystal, **F** is the external body force per unit mass and p is the pressure. The general form for the viscous stress tensor, $\tilde{t}_{ij}$, is given in the Appendix. A superposed dot represents the material time derivative, D/Dt, defined by

$$\frac{D}{Dt} = \frac{\partial}{\partial t} + v_i \frac{\partial}{\partial x_i}\,. \tag{10}$$

Similarly, from the general formulation, the angular momentum balance for the *c*-director leads, again in the absence of director gradients, to

$$-\frac{\partial w}{\partial c_i} + \tilde{g}^c_i + \tau c_i + \mu a_i = 0\,, \tag{11}$$

where the scalar functions τ and μ are Lagrange multipliers (arising from the aforementioned constraints on **a** and **c**). For this study, the energy density, w, consists of that related to the spontaneous polarisation only and is given, in terms of **a** and **c** [10], by

$$w = -\mathbf{P} \cdot \mathbf{E} = -P_0(\mathbf{a} \times \mathbf{c}) \cdot \mathbf{E} = -P_0 E \cos\phi \tag{12}$$

and therefore, in terms of the usual alternator ε_{ijk},

$$-\frac{\partial w}{\partial c_i} = -P_0 \varepsilon_{ijk} a_j E_k\,. \tag{13}$$

The dynamic contribution $\tilde{\mathbf{g}}^c$ is

$$\tilde{g}^c_i = -2\big(\lambda_2 D^c_i + \lambda_5 C_i + \tau_1 D^a_i + \tau_5 A_i\big), \tag{14}$$

where λ_2, λ_5, τ_1 and τ_5 are viscosity coefficients and the components A_i, C_i, D^a_i and D^c_i are given by

$$\begin{aligned} &A_i = \dot{a}_i - W_{ik}a_k\,, \quad C_i = \dot{c}_i - W_{ik}c_k\,, \\ &D^a_i = D_{ij}a_j\,, \quad D^c_i = D_{ij}c_j, \end{aligned} \tag{15}$$

where D_{ij} and W_{ij} are the usual rate of strain tensor and vorticity tensor, respectively, defined by

$$D_{ij} = \tfrac{1}{2}(v_{i,j} + v_{j,i})\,, \quad W_{ij} = \tfrac{1}{2}(v_{i,j} - v_{j,i})\,. \tag{16}$$

The vectors **A** and **C** are the co-rotational time fluxes for **a** and **c**, respectively. The main dynamic equations for the liquid crystal are, therefore, given by Equations 9 and 11, which will now be discussed in detail.

The external body force per unit mass of liquid crystal is $\mathbf{F} = -g\hat{\mathbf{z}}$ where g is the acceleration due to gravity. Noting that the divergence of the viscous stress is zero (because $\tilde{t}_{ij}$ does not contain any contributions that depend upon the spatial coordinates), straightforward calculations show that the equations in 9 are

$$\begin{aligned} &p_{,x} = 0, \quad p_{,y} = -\rho y\left(k^2(t) + \frac{dk}{dt}\right), \\ &p_{,z} = -\rho z\left(k^2(t) - \frac{dk}{dt}\right) - \rho g. \end{aligned} \tag{17}$$

These equations are solved by setting the pressure p to

$$\begin{aligned} p = &-\frac{1}{2}\frac{dk}{dt}\rho\big(y^2 - z^2\big) - \frac{1}{2}\rho\big(y^2 + z^2\big)k^2(t) \\ &+ \rho g(h_0 - z) + p_0\,, \end{aligned} \tag{18}$$

where p_0 is the force per unit area exerted by the upper boundary plate upon the fluid sample. When $t < 0$, $k \equiv 0$, $\phi \equiv \pi/2$ and $p = \rho g(h_0 - z) + p_0$. The solution 18 for p solves the linear momentum equations and it only remains at this stage to examine the angular momentum equations. For the forms stated in Equations 3–5 it is seen that, for **v** given by Equation 7,

$$\begin{aligned} &\mathbf{A} = \mathbf{0}\,, \quad \mathbf{C} = \frac{d\phi}{dt}(0, -\sin\phi, \cos\phi), \\ &\mathbf{D}^a = 0\,, \quad \mathbf{D}^c = k(t)(0, \cos\phi, -\sin\phi). \end{aligned} \tag{19}$$

With the aid of these results and Equation 13, it is seen that by taking the scalar product of Equation 11 with **a** that $\mu = -\tilde{\mathbf{g}}^c \cdot \mathbf{a}$ and, therefore, the first equation in Equation 11 is satisfied for this identified value of the multiplier μ. The remaining two equations from Equation 11, after appropriate substitutions using the results in Equations 13, 14 and 19, are

$$P_0E - 2\lambda_2 k(t)\cos\phi + 2\lambda_5\frac{d\phi}{dt}\sin\phi + \tau\cos\phi = 0, \tag{20}$$

$$2\lambda_2 k(t)\sin\phi - 2\lambda_5\frac{d\phi}{dt}\cos\phi + \tau\sin\phi = 0. \tag{21}$$

The multiplier τ can be eliminated from these expressions by multiplying Equation 20 by $\sin\phi$ and Equation 21 by $\cos\phi$ and subtracting, to leave the single equation

$$2\lambda_5\frac{d\phi}{dt} = -P_0E\sin\phi + 4\lambda_2 k(t)\sin\phi\cos\phi\,. \tag{22}$$

The three angular momentum equations in Equation 11, therefore, reduce to finding the solution of Equation 22. In summary, the liquid crystal dynamic Equations 9 and 11 effectively reduce to the solution of Equation 22 for the unknown functions $k(t)$ and $\phi(t)$.

The remaining equation that controls the motion of the system is that for the acceleration of the upper boundary plate. In the absence of director gradients, the stress tensor for the liquid crystal is [10, 11]

$$t_{ij} = -p\,\delta_{ij} + \tilde{t}_{ij} \tag{23}$$

and, therefore, adopting the standard convention for surface forces, the force per unit area exerted by the fluid upon the upper boundary plate is $t_i = t_{ij}\nu_j$, where $\boldsymbol{\nu}$ is the *inward* unit vector normal to the sample at the upper boundary and t_i is evaluated at $z = h_0 + h(t)$. Therefore, $t_i = -t_{i3}$ in this particular case. The only component of this force that is relevant to this model is the vertical force upon the plate, namely, $t_3 = -t_{33}$. The sum of this force exerted by the fluid upon the plate and the force exerted by the plate upon the fluid must be equal to the product of the mass per unit area of the upper boundary plate, ρ_p, multiplied by its acceleration $\ddot{h}(t)$, by Newton's second law. This is a legitimate approximation since the upper plate can be initially considered as floating on the fluid so that this buoyancy approach to the dynamics is valid (initially the pressure difference at the boundary interface is zero and the plate is at rest). Thus, at $z = h_0 + h(t)$, we have the moving boundary condition

$$\rho_p\frac{d^2h}{dt^2} = -t_{33} - p_0\,. \tag{24}$$

Inserting the quantities from Equations 16 and 19 into the viscous stress tensor, $\tilde{t}_{ij}$, stated in the Appendix shows that

$$\tilde{t}_{33} = -k(t)[\mu_0 + \mu_3\sin^2\phi(\sin^2\phi - \cos^2\phi) + 2\mu_4\sin^2\phi] + 2\lambda_2\frac{d\phi}{dt}\sin\phi\cos\phi. \tag{25}$$

Hence, by Equations 18, 23 and 25, the right-hand side of Equation 24 is

$$\begin{aligned} -t_{33} - p_0 = &-\frac{1}{2}\frac{dk}{dt}\rho(y^2 - z^2) - \frac{1}{2}\rho(y^2 + z^2)k^2(t) \\ &+ \rho g(h_0 - z) + k(t)[\mu_0 + \mu_3\sin^2\phi(\sin^2\phi - \cos^2\phi) \\ &+ 2\mu_4\sin^2\phi] - 2\lambda_2\frac{d\phi}{dt}\sin\phi\cos\phi\,, \end{aligned} \tag{26}$$

where the right-hand side is to be evaluated at $z = h_0 + h(t)$. However, $k(t)$ is connected to $h(t)$ via the relation 8 and thus the key two model Equations 22 and 26 can be expressed in terms of the two physically relevant unknown functions $\phi(t)$ and $h(t)$. Thus, upon making this substitution in Equation 26 for $k(t)$ in terms of $h(t)$ and its derivative and evaluating the expressions at $z = h_0 + h(t)$, Equation 26 becomes

$$\begin{aligned} -t_{33} - p_0 = &\frac{1}{2}\rho\left\{y^2[h_0 + h(t)]^{-1} - [h_0 + h(t)]\right\}\frac{d^2h}{dt^2} \\ &- \rho y^2[h_0 + h(t)]^{-2}\left(\frac{dh}{dt}\right)^2 - \frac{dh}{dt}[h_0 + h(t)]^{-1} \\ &\times [\mu_0 + \mu_3\sin^2\phi(\sin^2\phi - \cos^2\phi) + 2\mu_4\sin^2\phi] \\ &- 2\lambda_2\frac{d\phi}{dt}\sin\phi\cos\phi - \rho g h(t)\,. \end{aligned} \tag{27}$$

Each side of Equation 24 has dimensions of force per unit area. Both sides of this expression can be integrated over the region $0 \le x \le 1$, $-(w_0 - w(t))/2 \le y \le (w_0 - w(t))/2$, that is, over an area of unit length in the x-direction and of length $w_0 - w(t)$ in the y-direction, motivated by the geometry in Figure 2(b). Recall that the distance $w(t)$ can be expressed in terms of $h(t)$ via the relation 2 and so $w_0 - w(t) = w_0h_0/(h_0 + h(t))$. Substituting Equation 27 into 24, carrying out this integration and then dividing both sides by $w_0 - w(t)$ leads to

$$\begin{aligned} \rho_p\frac{d^2h}{dt^2} = &\frac{1}{2}\rho\{\frac{1}{12}w_0^2h_0^2[h_0 + h(t)]^{-3} - [h_0 + h(t)]\ \frac{d^2h}{dt^2}\} \\ &- \frac{1}{12}\rho w_0^2h_0^2[h_0 + h(t)]^{-4}\left(\frac{dh}{dt}\right)^2 \\ &- \frac{dh}{dt}[h_0 + h(t)]^{-1}[\mu_0 + \mu_3\sin^2\phi(\sin^2\phi - \cos^2\phi) \\ &+ 2\mu_4\sin^2\phi]\ - 2\lambda_2\frac{d\phi}{dt}\sin\phi\cos\phi - \rho g h(t)\,. \end{aligned} \tag{28}$$

Finally, substitution for $k(t)$ in terms of h in Equation 22 gives

$$2\lambda_5 \frac{d\phi}{dt} = -P_0 E \sin\phi - 4\lambda_2 \frac{dh}{dt}[h_0 + h(t)]^{-1} \sin\phi\cos\phi. \quad (29)$$

Thus the two coupled dynamic equations that need to be solved for $\phi(t)$ and $h(t)$ are given by Equations 28 and 29 and it is these Equations that we consider in the next section.

4. Solutions

Equations 28 and 29 have been solved numerically using Maple [17] for the typical material parameters listed in Table 1. The initial conditions were first set to be

$$\phi(0) = 3.141 \text{ rad}, \qquad h(0) = 0, \qquad \frac{dh}{dt} = 0, \quad (30)$$

motivated by the initial configuration pictured and discussed in Figure 1(c). An initial small displacement to the $\phi \equiv \pi$ state has been presupposed in order to initiate a small perturbation to generate a non-constant solution. The field, E, is then set to 10^6 V m^{-1} for these conditions and solved numerically. The results are shown in Figure 3.

As perhaps expected, the orientation angle ϕ tends to zero as the spontaneous polarisation aligns with the direction of the field, as shown in Figure 3(a). The corresponding displacement $h(t)$ and acceleration d^2h/dt^2 of the upper plate are plotted in Figures 3(b) and (c). The system approaches its new equilibrium state within a timescale of around 1 ms, which is in agreement with the observed timescales reported in [7]. The displacement $h(t)$ of the upper plate settles to a positive value, indicating that there is an increase to the sample depth after the electric field is suddenly reversed and maintained. Also, there is an initial positive acceleration of the plate which then reverses sign before tending to zero. This matches the qualitative behaviour for the experimental acceleration given in [4, 7], although the data in these articles had decaying periodic oscillations occurring over the same timescale as that presented in Figure 3(c). There are, therefore, two features in this present model that are of importance: the first is the increase in sample thickness through a reversed field and the second is the behaviour of the acceleration of the plate. An increase in sample thickness can, therefore, be modelled within the context of the continuum theory used here. Although the increase in h in Figure 3(b) is small (of the order 10^{-9} m), it is nevertheless significant, as will be discussed later when an alternating field is considered.

It is natural at this point to consider an initial state with the field reversed from the stated value of E to $-E$ when $\phi \equiv 0$ and the other initial conditions remain as in Equation 30. As before, a small initial disturbance to the orientation angle is required to initiate a non-constant solution and so $\phi(0) = 0.001$ rad was used in the numerical calculations. The results are shown in Figure 4 and the timescale for ϕ and h to reach their equilibrium states is the same as in Figure 3.

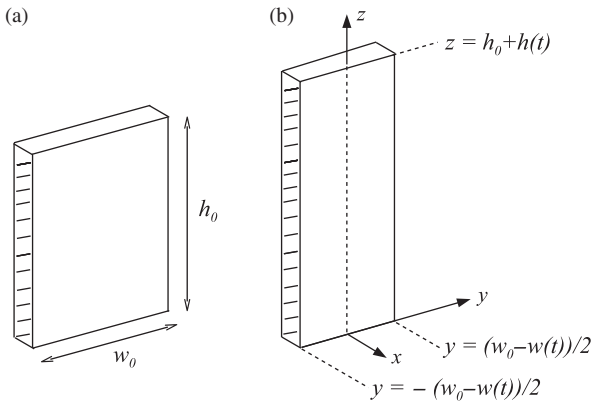

Figure 2. The geometrical description of a single representative SmC* layer under a fast electric field reversal. (a) At $t = 0$ the representative incompressible layer has height h_0 and width w_0. (b) Under a field reversal the top plate may move, leading to a change in shape of the sample. To maintain a fixed volume of fluid the area of the representative layer must effectively remain constant for incompressible SmC*. Any increase in the height must be accompanied by a corresponding decrease in the width so that the relation in Equation 2 holds.

Table 1. Typical material parameters discussed in the text and used in numerical calculations. The values for h_0, w_0, P_0 and E have been taken from Jákli and Saupe [7]. The viscosity coefficients have been estimated from data available for smectic liquid crystals and have been selected to ensure that basic *a priori* inequalities that involve combinations of viscosities have been satisfied [10, pp 300–301]. The density ρ is typical for a liquid crystal while ρ_p has been based on an estimate of 30 g for the total mass of an upper plate of area 9 cm^2, as used in [7].

Parameter	Typical value
h_0	5×10^{-6} m
w_0	3×10^{-2} m
P_0	10^{-3} C m^{-2}
E	10^6 V m^{-1}
μ_0	0.0400 Pa s
μ_3	0.0200 Pa s
μ_4	0.1083 Pa s
λ_2	0.0625 Pa s
λ_5	0.0300 Pa s
ρ	1020 kg m^{-3}
ρ_p	33 kg m^{-2}

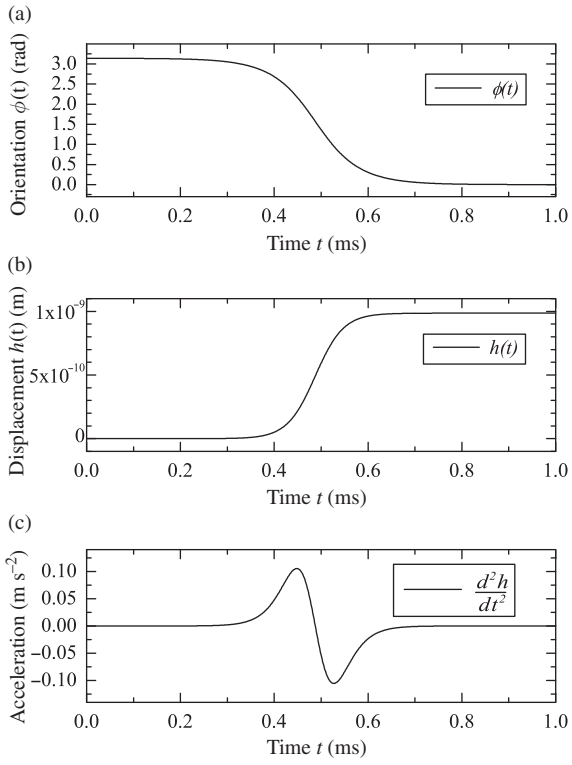

Figure 3. Solutions to Equations 28 and 29 for the orientation angle, $\phi(t)$, of the c-director and displacement $h(t)$ of the upper boundary plate subject to the initial conditions in Equation 30 and the parameters listed in Table 1. (a) $\phi(t)$ tends to the zero equilibrium state in around 1 ms. (b) $h(t)$ increases and reaches a steady state within 1 ms. (c) The acceleration of the upper plate.

Through a similar mechanism, the c-director orientation angle, ϕ, tends to π so that the spontaneous polarisation aligns with the field. However, there is a positive increase in the sample depth and the acceleration of the upper plate is very similar to that in Figure 3. This may mean that a continued periodic reversal of the field will induce a periodic oscillation of the polarisation and a continuous increase in the sample thickness, that is, an oscillating field could cause a build-up in sample thickness. Therefore, an increase in the sample thickness does not depend on the direction of the field reversal: this important feature was also noted by Jákli and Saupe [7], despite their observation of an initial decrease before an increase in the thickness (possibly due to the sample being close to the SmC*–SmA transition temperature) that was independent of the field direction. An increase in sample thickness induced by critical oscillating electric fields while the smectic interlayer spacing remains constant has been reported in [6] and the results presented here show that this may well be feasible within the present basic model. After a period of time, the sample thickness may increase significantly, as has been observed experimentally in [6]. The present theoretical model supports this observation and demonstrates that it can be driven by flow coupled to the reorientation of the spontaneous polarisation.

With this in mind, after some elementary experimentation with an alternating field of the form

$$\mathbf{E} = E\cos(2\pi ft)\hat{\mathbf{z}}, \tag{31}$$

with $f = 320$ Hz and the initial conditions and parameter values given in Equation 30 and Table 1, solutions to Equations 28 and 29 for ϕ, h and the acceleration of the upper plate were evaluated numerically. The value for f is close to that used for the model in [6]. The results are presented in Figure 5; many

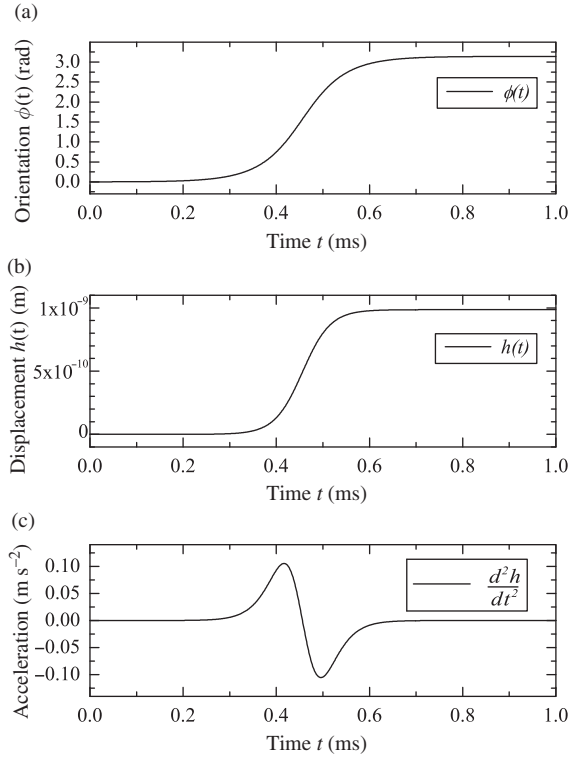

Figure 4. Solutions to Equations 28 and 29 for the orientation angle $\phi(t)$ of the c-director and displacement $h(t)$ of the upper boundary plate subject to the same initial conditions as in Equation 30 for $h(t)$ but now with $\phi(0) = 0.001$ rad. The parameters listed in Table 1 were used except that here the electric field has been reversed to $E = -10^{-6}$ V m^{-1}. (a) $\phi(t)$ tends to the equilibrium state π in around 1 ms. (b) $h(t)$ increases and reaches a steady state within 1 ms. (c) The acceleration of the upper plate. The results in (b) and (c) are very similar to the corresponding results in Figure 3, despite a reversal in the sign of the electric field.

similar plots can be determined for various sets of material parameters and initial conditions.

The plot in Figure 5(a) shows that the polarisation tends to its original orientation while, as predicted from the previous results, the displacement of the upper plate, shown in Figure 5(b), continues to increase steadily in a pumping fashion and, moreover, approaches a constant equilibrium value at about 20 ms. The graph of the acceleration of the upper plate, d^2h/dt^2, appears in Figure 5(c) and has the same qualitative behaviour as the data plots from experiments for a fast field reversal, presented in [4, 7], except that the magnitude of the acceleration is much smaller in what appears here. The crucial feature is really the steady increase in the sample thickness until it reaches a positive equilibrium state as presented in Figure 5(b). This phenomenon is qualitatively what is known to happen in SmC* samples in this geometry as reported by Jákli and Saupe [6] and occurs under oscillating low-frequency electric fields: there is a steady growth in the sample thickness until it reaches an increased constant depth. Although the predicted eventual displacement in Figure 5(b) is relatively small, it is qualitatively similar to the experimental results. In [6], the final displacement for a sample of initial depth 8 μm was about 300 nm and this is about one order of magnitude greater than that predicted in Figure 5(b). The basic theoretical model in [6] cannot explain this phenomenon and it is only when the rotation of the spontaneous polarisation is coupled to flow that it can be detected theoretically, as has just been demonstrated.

The time taken for the displacement, $h(t)$, to reach its positive equilibrium state will vary as the amplitude and frequency of the field varies. The influence of the material parameters will also be crucial. All these factors will contribute to the final value for the vertical displacement, $h(t)$, that is induced by this pumping phenomenon. More realistic fits with experimental data may be possible by extending the model equations, for example, to include smectic elastic constants, anchoring conditions and the surface tension at the vertical walls of the sample, or by taking a more sophisticated approach to the modelling of the velocity. The pumping effect is particularly sensitive to the frequency of the electric field. Experimentally, there is a critical frequency, f_c, at which the onset of pumping occurs and the upper plate begins to rise [6]. A theoretical determination of f_c has been given by Carlsson and Stewart [8] and the value of $f = 320$ Hz used in Figure 5 is known to be above this threshold for similar material parameters. The model in [8] also incorporated elastic effects and strong anchoring conditions on the director at the boundaries in order to obtain f_c, but the approach involved coupled linearised equations and could only detect the onset of pumping and could not model the increase in the field-induced thickness changes that occur for $f > f_c$.

For the parameters used to obtain the results in Figure 5, it is, nevertheless, possible to gain some insight into the influence of the frequency of the alternating field used in Equation 31. It would appear from the numerical results that the displacement $h(t)$ approaches its final equilibrium state within a timescale of about 20 ms. Solutions for different frequencies can be calculated and then evaluated at $t = 20$ ms in order to obtain a feasible estimate for the dependence of the final boundary plate displacement upon the frequency. The result is shown in Figure 6.

It is clear that the eventual displacement in h is frequency dependent, as is known from experiments [6]. Moreover, this particular system is more sensitive

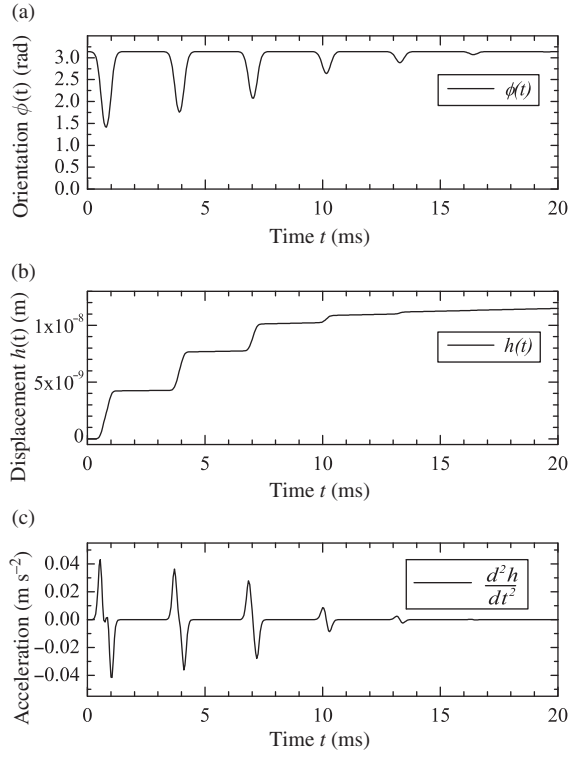

Figure 5. Solutions to Equations 28 and 29 for the orientation angle $\phi(t)$ of the c-director and displacement $h(t)$ of the upper boundary plate subject to the initial conditions in Equation 30. The parameters listed in Table 1 were used except that here the electric field has been replaced by the alternating field stated in Equation 31. (a) $\phi(t)$ manoeuvres to maintain its equilibrium state π and achieves its steady state after around 20 ms. (b) $h(t)$ steadily increases and reaches a steady state within 20 ms. (c) The acceleration of the upper plate. These results show that there is a pumping phenomenon that drives a steady increase in the sample thickness through increases in the boundary displacement, $h(t)$.

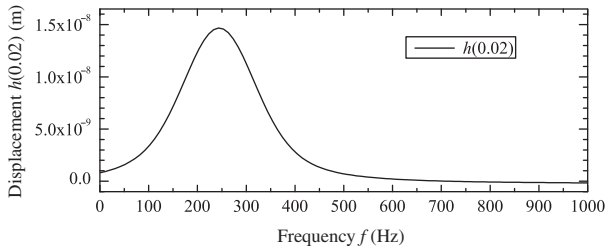

Figure 6. The dependence of the displacement h of the upper boundary plate evaluated at $t = 20$ ms as the frequency f of the electric field is varied.

to lower frequencies and this, again, is in accord with experimental observations [6] and previous theoretical results [8].

5. Discussion

This article has derived governing equations that can model a field-induced pumping phenomenon in SmC* liquid crystals when the upper boundary plate of a bookshelf aligned sample is free to move. The main dynamic Equations 28 and 29 were solved numerically for the typical material parameters in Table 1 and displayed in Figures 3–6. In a simple sudden electric field reversal the director reorients through π rad as the spontaneous polarisation aligns with the field and this is accompanied by a small increase in the sample thickness and a small vibration to the upper boundary, as shown in Figures 3 and 4, an increase that is independent of the direction of the field. When an alternating field is applied the director can reorient and tend to its original position accompanied by mechanical vibrations of the upper plate and a steady rise in the sample thickness. It is this steady increase that is of importance because it demonstrates theoretically the possibility of a pumping effect where there is a build-up in sample thickness as the upper plate continuously rises to a new equilibrium level that is maintained under the application of an alternating field. This phenomenon is in accord with the experimental observations of Jákli and Saupe [6], whose preliminary model could not account for this mechanical behaviour but whose data revealed a vertical displacement of the upper plate at a voltage of $V \simeq h_0 E = 5$ V, as used here. These vertical displacements are in qualitative agreement with the theoretical predictions for $h(t)$ in Figures 3–5. The pumping effect is sensitive to the frequency of the alternating field and the dependence of an approximation to the final boundary displacement upon the frequency has been shown in Figure 6. Further, the pumping effect under a simple fast field reversal, such as that applied here, is known to occur over timescales of the order of 1 ms [7] and this is compatible with the model results presented in Figures 3 and 4. One discrepancy in this model in relation to experimental evidence is the magnitude of the acceleration of the upper boundary under a field reversal. As mentioned in Section 4, this may be due to approximating conditions that have been implemented in this work. Surface tension at the vertical sides of the sample and anchoring conditions for the director on the boundaries, which have been neglected here, will play prominent roles. However, there are two approximations that were introduced that have possibly been more influential on the results: the first was to neglect the elasticity of the liquid crystal because of the reported dominance of viscous effects [2] and the second was to invoke a particular ansatz for the velocity. The flow component in the y-direction possibly needs a more elaborate ansatz, or perhaps the velocity could be determined in a more precise way through what will obviously be quite substantially more complicated dynamic equations. Modification of these two particular assumptions should be seen as the next step towards a more refined model. In any event, the analysis in this article should be seen as a first basic approach that captures some of the essential experimental features and it is clear that the problem deserves to be investigated in a more sophisticated manner.

One feature worth commenting on is the role of the viscosity coefficient λ_2. Experimental values for λ_2 are only known in relation to combinations of other viscosities [10, 18, 19]. The sign of this viscosity could be positive or negative and may depend on the particular material (it is well-known in nematic liquid crystals, for example, that some viscosity coefficients have different signs for different materials). It has been seen that the pumping phenomenon occurs for $\lambda_2 > 0$; however, when the numerical procedures are repeated for values of λ_2 that are negative yet remain consistent with all the necessary *a priori* inequalities in relation to the other viscosities, the pumping phenomenon may lead to a decrease in the sample thickness or, in many instances, to solutions for $h(t)$ that fail to be determined beyond a very short time interval. It would appear that a positive value for λ_2 encourages a steady increase in the sample thickness under oscillating electric fields. Changes to the other viscosities do not have such a dramatic effect.

One major difference in the modelling of field-induced sample thickness changes used by Jakli [4] and Jákli and Saupe [7] is a proposed expansion and contraction in the smectic interlayer spacing. In common with the models introduced in [5, 6] and in agreement with the incompressible continuum smectic theory [10, 11], changes in the smectic interlayer spacing were not supposed in this article. The introduction of

such interlayer changes may be modelled by a more extensive continuum theory that allows compressibility of the layers, such as that recently introduced for smectic A liquid crystals [20]. This may lead to a more intricate analysis of general pumping phenomena in smectic liquid crystals.

As noted in [4], electric field-induced mechanical vibrations and related effects may have practical applications in the area of electromechanical transducers which can form the key elements of possible intelligent materials [21]. The pumping effect in ferroelectric liquid crystals can also be used in micromanipulation methods. Using backflow in a ferroelectric liquid crystal and adjusting the polarity and frequency of an applied electric field, a net movement of microparticles has been achieved by Mieda and Furutani [22, 23]. Such micromanipulation techniques may be suitable for the precise manipulation of microparticles that would otherwise be difficult to manoeuvre, such as microlenses or micro-mirrors [23]. The motion of single micrometre-sized glass spheres in SmC* liquid crystals was investigated experimentally by Dierking *et al.* [24], who described the electromigration of such particles as almost certainly caused by backflow, possibly due to a mass pumping phenomenon. It is perhaps also worth adding that, in the context of ferroelectric liquid crystalline elastomers, Madden *et al.* [25] have written a review that discusses the electrically-induced displacements of these materials in the area of possible actuator technologies.

Acknowledgements

The author is grateful to the late Professor Alfred Saupe for introducing him to the phenomenon of pumping in ferroelectric liquid crystals during a visit to the Max Planck Research Group for Liquid Crystal Systems, Martin Luther University Halle-Wittenberg, Germany. He also wishes to thank Dr. T. Carlsson for many stimulating conversations on the dynamics of liquid crystals.

References

[1] Clark, N.A.; Lagerwall, S.T. *Appl. Phys. Lett.* **1980**, *36*, 899–901.
[2] Jákli, A.; Bata, L.; Buka, Á.; Éber, N.; Jánossy, I. *J. Phys. Lett. (Paris)* **1985**, *46*, L759–L761.
[3] Jákli, A.; Saupe, A. *Liq. Cryst.* **1991**, *9*, 519–526.
[4] Jákli, A. *Mol. Cryst. Liq. Cryst.* **1997**, *292*, 293–300.
[5] Zou, Z.; Clark, N. *Phys. Rev. Lett.* **1995**, *75*, 1799–1802.
[6] Jákli, A.; Saupe, A. *Phys. Rev. E: Stat., Nonlinear, Soft Matter Phys.* **1996**, *53*, R5580–R5583.
[7] Jákli, A.; Saupe, A. *Mol. Cryst. Liq. Cryst.* **1995**, *263*, 103–111.
[8] Carlsson, T.; Stewart, I.W. Pumping in ferroelectric smectic liquid crystals. To be submitted for publication.
[9] de Gennes, P.G.; Prost, J. *The Physics of Liquid Crystals*, 2nd ed.; Oxford University Press: Oxford, 1993.
[10] Stewart, I.W. *The Static and Dynamic Continuum Theory of Liquid Crystals*; Taylor and Francis: London and New York, 2004.
[11] Leslie, F.M.; Stewart, I.W.; Nakagawa, M. *Mol. Cryst. Liq. Cryst.* **1991**, *198*, 443–454.
[12] Clark, N.A.; Lagerwall, S.T. *Ferroelectrics* **1984**, *59*, 25–67.
[13] Oseen, C.W. *Trans. Faraday Soc.* **1933**, *29*, 883–899.
[14] Carlsson, T.; Leslie, F.M.; Clark, N.A. *Phys. Rev. E: Stat., Nonlinear, Soft Matter Phys.* **1995**, *51*, 4509–4525.
[15] Leslie, F.M. *Liquid Crystal Devices*; Instituut Wiskundige Dienstverlening, Technische Universiteit Eindhoven, 1992.
[16] Clark, M.G.; Saunders, F.C.; Shanks, I.A.; Leslie, F.M. *Mol. Cryst. Liq. Cryst.* **1981**, *70*, 195–222.
[17] *Maple 11*; Waterloo Maple Inc., 2007.
[18] Galerne, Y.; Martinand, J.L.; Durand, G.; Veyssie, M. *Phys. Rev. Lett.* **1972**, *29*, 562–564.
[19] Leslie, F.M. *Liq. Cryst.* **1993**, *14*, 121–130.
[20] Stewart, I.W. *Continuum Mech. Thermodyn.* **2007**, *18*, 343–360.
[21] Rogers, C.A. *Scientific American* **2003**, *9*, 122–127.
[22] Mieda, Y.; Furutani, K. *Phys. Rev. Lett.* **2005**, *95*, 177801.
[23] Mieda, Y.; Furutani, K. In *2006 IEEE International Symposium on Micro-NanoMechatronics and Human Science*; Nagoya, Japan, November 6–8, 2006; pp 208–213.
[24] Dierking, I.; Cass, P.; Syres, K.; Cresswell, R.; Morton, S. *Phys. Rev. E: Stat., Nonlinear, Soft Matter Phys.* **2007**, *76*, 21707.
[25] Madden, J.D.W.; Vandesteeg, N.A.; Anquetil, P.A.; Madden, P.G.A.; Takshi, A.; Pytel, R.Z.; Lafontaine, S.R.; Wieringa, P.A.; Hunter, I.W. *IEEE J. Oceanic Eng.* **2004**, *29*, 706–728.

Appendix

The general expression for the viscous stress, $\tilde{t}_{ij}$, for the SmC* phase can be written as

$$\tilde{t}_{ij} = \tilde{t}^{s}_{ij} + \tilde{t}^{ss}_{ij}, \tag{A.1}$$

where $\tilde{t}^{s}_{ij}$ and $\tilde{t}^{ss}_{ij}$ are the symmetric and skew-symmetric parts of the viscous stress given by [10, 11]

$$\begin{aligned}\tilde{t}^{s}_{ij} = {} & \mu_0 D_{ij} + \mu_1 a_p D^a_p a_i a_j + \mu_2 (D^a_i a_j + D^a_j a_i) \\ & + \mu_3 c_p D^c_p c_i c_j \ + \mu_4 (D^c_i c_j + D^c_j c_i) \\ & + \mu_5 c_p D^a_p (a_i c_j + a_j c_i) \ + \lambda_1 (A_i a_j + A_j a_i) \\ & + \lambda_2 (C_i c_j + C_j c_i) + \lambda_3 c_p A_p (a_i c_j + a_j c_i) \\ & + \kappa_1 (D^a_i c_j + D^a_j c_i + D^c_i a_j + D^c_j a_i) \\ & + \kappa_2 [a_p D^a_p (a_i c_j + a_j c_i) + 2 a_p D^c_p a_i a_j] \\ & + \kappa_3 [c_p D^c_p (a_i c_j + a_j c_i) + 2 a_p D^c_p c_i c_j] \\ & + \tau_1 (C_i a_j + C_j a_i) + \tau_2 (A_i c_j + A_j c_i) \\ & + 2\tau_3 c_p A_p a_i a_j + 2\tau_4 c_p A_p c_i c_j,\end{aligned} \tag{A.2}$$

$$\begin{aligned}\tilde{t}_{ij}^{ss} = {} & \lambda_1(D_j^a a_i - D_i^a a_j) + \lambda_2(D_j^c c_i - D_i^c c_j) \\ & + \lambda_3 c_p D_p^a (a_i c_j - a_j c_i) \ + \lambda_4 (A_j a_i - A_i a_j) \\ & + \lambda_5 (C_j c_i - C_i c_j) + \lambda_6 c_p A_p (a_i c_j - a_j c_i) \\ & + \tau_1 (D_j^a c_i - D_i^a c_j) + \tau_2 (D_j^c a_i - D_i^c a_j) \\ & + \tau_3 a_p D_p^a (a_i c_j - a_j c_i) \ + \tau_4 c_p D_p^c (a_i c_j - a_j c_i) \\ & + \tau_5 (A_j c_i - A_i c_j + C_j a_i - C_i a_j).\end{aligned} \tag{A.3}$$

The quantities A_i, C_i, D_i^a and D_i^c are defined through the relations in Equations 15 and 16. There are 20 viscosity coefficients: the 12 viscosities μ_0 to μ_5 and λ_1 to λ_6 are associated with contributions to the dynamic stress which are even in the vector **c** or do not contain **c**, while the remaining eight viscosities κ_1 to κ_3 and τ_1 to τ_5 are linked to the terms which are odd in the vector **c**. The viscosity μ_0 is related to the usual isotropic Newtonian viscosity η through the relation $\eta = \frac{1}{2}\mu_0$.